Multiphase Science and Technology, Vol. 17, Nos. 1-4, pp. 1-13, 2005

REMARKS ON THE DISTRIBUTION OF INERTIAL PARTICLES IN THE WALL REGION OF A TURBULENT BOUNDARY LAYER

Maurizio Picciotto, Cristian Marchioli and Alfredo Soldati*
Centro Interdipartimentale di Fluidodinamics e Idraulica, Dipartimento di Energetica e Macchine, Università degli Studi di Udine, Via delle Scienze 208, 33100 Udine, Italy

Abstract. The problem of particle preferential distribution in turbulent boundary layer is addressed.l Several observations confirm that, in this type of flow, particles have a non-uniform distribution in the wall normal direction and it has also been observed that, when in the viscous sub-layer, particle distribution is not uniform in the wall parallel plane so that particles appear segregated along streamwise streaks with strong time persistency. Starting from our previous works [1, 2, 3], in which we examined the mechanisms for particle transfer toward and away from the wall, we aim at characterizing the regions of particle preferential distribution. Particle motion in the wall region is deminated by instantaneous Reynolds stresses – i.e. strong downwash of outer fluid toward the wall, sweeps, and strong upwash of fluid away from the wall, ejections – which are generated by the coherent vortical structures populating the wall region.

Specifically, in this work we correlate particle preferential position with the distribution of the coherent structures in the wall region. Results confirm that particles tend to avoid the strongly coherent vortifcal structures and tend to concentrate in regions neighbouring the wall which are characterized by low shear stress values where the flow is generally directed aay from the wall.

Keywords: Direct Numerical Simulation, Lagrangian Tracking, Turbulent Boundary Layer, Coherent Structures, Deposition, Preferential Distribution, Re-entrainment.

1. INTRODUCTION AND BACKGROUND

* Author to whom correspondence should be addressed: soldati@uniud.it

Particle transfer in the wall region of a turbulent boundary layer is a highly nonuniform and intermittent phenomenon which depends on the local dynamics of turbulence structures. Decades of extensive studies have clarified several issues concerning the relationship between turbulence structures and particle dynamics [1, 4, 5, 6]. To resume several of those, we refer to our previous works [1, 2, 3] in which the causal relationship between turbulence structures and particle transfer mechanisms is addressed. A representative view of particle dynamics and distribution in a turbulent boundary layer is shown in Figure 1a. In this figure a cross-sectional view of particle instantaneous distribution in the half domain of an upward turbulent channel flow. The snapshot is taken at the dimensionless simulation time $t^+ = 2700$. In this work, we use the superscript "+" to identify wall units, i.e. variables made dimensionless by using viscosity, ν, and friction velocity $u_\tau = (\tau_w/\rho)^{1/2}$, where τ_w is wall shear stress and ρ is fluid density. In Figure 1a, the flow is directed toward the reader and particles with relaxation time τ_p^+ equal to 116.3 are considered. Particle relaxation time is defined as $\tau_p = \rho_p d_p^2/18\mu$, where ρ_p, d_p and μ are particle density, particle diameter and fluid dynamic viscosity respectively. Figure 1a shows a number of features which can classify the process of particle dispersion and transfer in turbulent boundary layer. First, we can observe that particles are not homogeneously distributed along the channel, but they tend to cluster. In particular, particles tend to cluster around the larger vortical structures. From these clusters, particles are transported toward the wall, where they accumulate in specific "reservoirs" (one of these is indicated by the black circle) where concentration build-up occurs. These accumulation regions are classified by flow streamwise velocity lower than the mean (see also [4, 5] among others). Particles tend to stay long times in these low-speed regions so that eventually particle concentration increases near the wall. To quantify near-wall accumulation, the particle number density distribution is plotted as a function of the non dimensional distance z^+ from the wall in Figure 1b. A logarithmic scale is used to capture the detail of particle behaviour in the proximity of the wall. The concentration profile is developing with time, and at the instant captured in Figure 1b, we ob serve that particle number density profile has developed a maximum well into the near-wall region ($0 < z^+ < 20$). This behaviour can be viewed as the consequence of the turbulence non homogeneity [3, 7], and has been observed in a number of previous works [2, 8, 9].

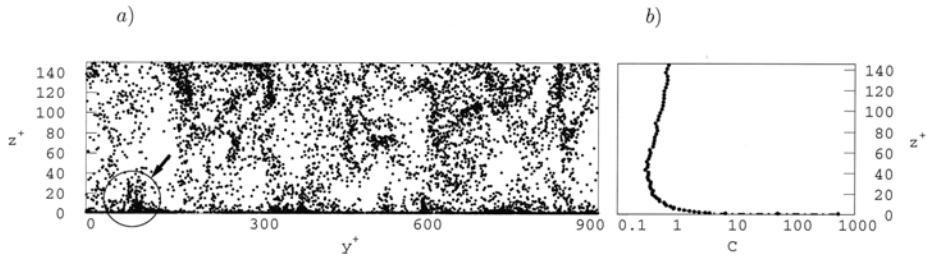

Figure 1 Instantaneous distribution of particles characterized by $\tau_p^+ = 116.3$ at time $t^+ = 2700$. View of particle position in the yz-plane for $700 < x^+ < 1000$ (a) and corresponding xy-plane average number density distribution as a function of the wall normal direction (b).

Particle transfer processes are dominated by the dynamics of turbulent structures in the wall proximity. We refer to previous works ([10, 11, 12]) for details and explanations, and we will quickly review here some of the main phenomena occurring near the wall. The near-wall region is characterized by streamwise "streaks" of fluid with velocity lower than the mean alternated with regions of velocity higher than the mean. The "low-speed" streaks are the footprint of the counter-rotating coherent quasi-streamwise vortices, which populate the near-wall region [13]. These vortices line up as a staggered array and are slightly tilted upward so that the forward end of a vortex stands above the rear end of the preceding vortex. The scenario is depicted in Figure 2: the forward end of a vortex generates in-sweeps of high momentum fluid on its downwash side and ejections of low momentum fluid on its upwash side. Low-speed streaks are also seen as the production of series of low momentum fluid ejections. The sweeps and ejections are instantaneous realizations of the Reynolds stresses: the strong coherent sweeps drive particles toward the wall whereas ejections drive particles away from the wall [1, 14]. Qualitative examination of the mechanisms which control particle deposition and resuspension [1] showed that the rear end of the preceding vortex prevents a large fraction of particles in the proximity of the wall from being resuspended. Specifically, particles brought by the sweeps in the high speed region would tend to loop around the quasi streamwise vortex. However, particles are transported to the wall mostly by strongly coherent sweeps, which in turn are generated in proximity of the forward end of the quasi streamwise vortices. Thus, once coming from the wall region and approaching the ejection area, particles feel the counter action of the rear-end of the preceding counter-rotating vortex. Since vortices are tilted upward

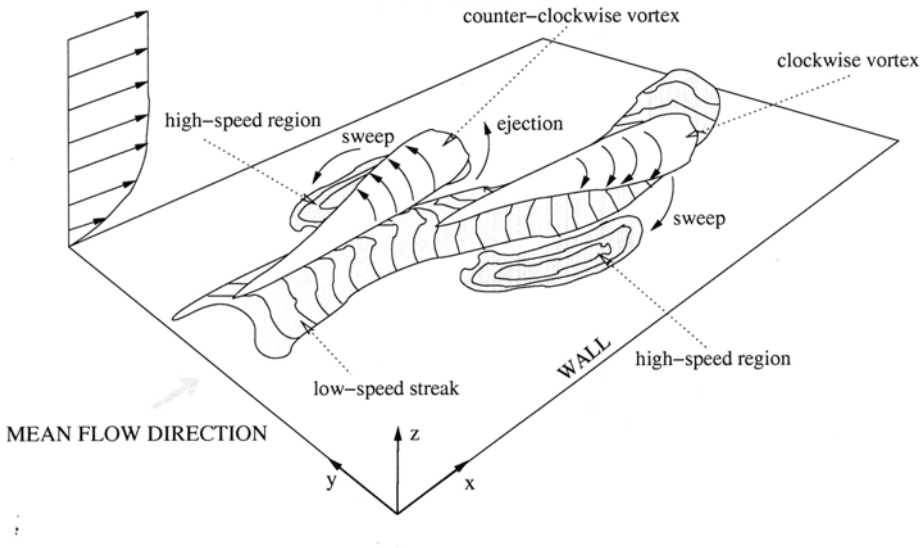

Figure 2 Minimal schematics of wall turbulence phenomena dynamics. Strong causal relationship exists which links low-speed streaks to ejections generated by quasi-streamwise vortices, which also generate sweps which bring high streamwise momentum fluid to the wall in the high velocity regions.

in the streamwise direction, the rear end of the preceding vortex is well into the viscous sublayer and prevents particles to reach the area where the strong ejection generated by the forward end of the following vortex is taking place. As a consequence, particle transfer toward the wall is more efficient than particle transfer away from the wall and nonuniform particle concentration occurs, which peaks close to the wall (*turbophoresis*, see [1, 7]).

The object of this work is to elaborate on the scenario depicted in on previous papers [1, 3] providing quantitative information on particle distribution in the wall region of a turbulent boundary layer. Specifically, we will investigate on the relationship between particle distribution and flow topology as discussed by [15]. Finally, we will demonstrate the role of specific critical flow regions at the wall in attracting and segregating particles.

For the numerical experiments, we used the same methodology discussed in [1]. Particles are introduced in a numerically simulated turbulent Poiseuille flow of air (incompressible and Newtonian) at $\mathrm{Re}_\tau = u_\tau h/\nu = 150$, where h is the channel half-width. The reference geometry consists of two infinite vertical flat parallel walls: periodic boundary conditions are imposed on the fluid velocity field both in streamwise (x) and spanwise (y) directions and no-slip boundary conditions are imposed at the walls. The computational domain is $1885 \times 942 \times 300$ wall units in x, y and z with $64 \times 64 \times 65$ nodes. The time step used for the fluid was $\Delta t^+ = 0.35325$ in wall time units. We assume that particle number density and particle size are both small: the feedback of the particles onto the gas flow is negligible. Particles are assumed to be pointwise, rigid, spherical and their Lagrangian equation of motion includes the effects of particle inertia, Stokes drag and Saffman lift force. We considered both the case of upward flow (gravity opposed to flow direction) and the case of no gravity. Results presented in the following refer to the upward case unless otherwise indicated. Three sets of 48^3 flyash particles ($\tau_p^+ = 3.8, 29.1, 116.3$) were initially released at random locations within the computational box. We considered that a particle is elastically reflected away from the wall when its center is less than a distance $D_p/2$ from the wall.

2. RESULTS AND DISCUSSION

As already observed [6, 16, 17] particle position in the wall region correlates well with low-speed streaks, which are characterized by negative values of the streamwise velocity fluctuation, u'. Even though low-speed streaks are ejection-like environments, most of the particles do not leave the wall region but rather, they remain trapped for long time. Since particle transfer fluxes are strongly dominated by large-scale vortical structures [1, 15], we analyzed the correlation between these structures and particle position. In our previous work [1], we examined the dynamics of single structures in correlation with particle dynamics and we produced a qualitative mechanism for particle transfer. In this work, we will use global identifiers to correlate particle distribution with coherent structures on a statistical base.

In particular, we related particle non-homogeneous accumulation to coherent flow structures, according to the general classification scheme proposed by [18] and [19]. This classification scheme groups all elementary three-dimensional flow patterns and is based on the three invariants of the velocity gradient tensor u_{ij}:

$$P = u_{i,i}, \tag{1}$$

$$Q = \frac{1}{2}\left[(u_{i,i})^2 - u_{i,j}u_{j,i} \right] = -\frac{1}{2}u_{i,j}u_{j,i} = \frac{1}{2}(\Omega_{ij}\Omega_{ij} - S_{ij}S_{ij}) \tag{2}$$

$$R = -\lambda_1\lambda_2\lambda_3, \tag{3}$$

where the RHS of eq. (2) holds for incompressible flow fields. Here $\Omega_{ij} = ½(u_{i,j} - u_{j,i})$ and $S_{ij} = ½(u_{i,j} - u_{j,i})$ are the antisymmetric and symmetric components of the velocity gradient whereas λ_1, λ_2 and λ_3 are the eigenvalues of $u_{i,j}$. The velocity gradient tensor has been widely used to describe typical local deformations of fluid elements. Its invariants determine, for instance, if the deformations produce vorticity stretching along a specific direction (possibly yielding tubular vortices) or if they produce structures that are flattened out in one direction while expanding in the other two (possibly yielding pancake-like structures). In an effort to give a physical insight, we can consider as an example the quantity Q. Limited to incompressible flows, Q may represent the local balance between vorticity (related to Ω_{ij}) and the strain rate (related to S_{ij}). Thus, a fluid point characterized by positive values of Q indicates the presence of high vorticity, whereas for negative values of Q the local flow is dominated by straining motions [20].

For clarity of presentation, in Figure 3 we show all incompressible flow topologies using the (Q,R)-plane [19]. Four regions can be identified: two vortical flow regions, the so-called stable focus/stretching (*I*) and unstable focus/compressing (*II*), and two convergence regions, the so-called stable node/saddle/saddle (*iii*) and unstable node/ saddle/saddle critical nodes (*IV*). Further critical points can be identified along the Q-axis and the $D = 0$ line: the so-called center/no flow (α), stable star node/saddle/saddle (β), stable line node-saddle/unstable line node-saddle/no flow (γ) and unstable star node/saddle/saddle (δ). It is beyond the scope of this paper to map the flow topologies characterizing the viscous sublayer: we will exploit the classification system only to elucidate the relationship between particle distribution and near-wall vortices.

Following [15], we computed Q and R for the fluid at each grid point in the viscous sublayer. Then, we conditionally sampled Q and R at particle position to determine whether particles show preference for or against any of the aforementioned topologies. Figure 4 shows the resulting joint probability density function (PDF) of Q and R in the viscous sublayer. PDFs were calculated over 400 instants of the flow field to consider only those events with significant statistical occurrence. As reported in [15], the most probable value of Q ad R is zero for all the instants. The PDF sampled for the fluid at grid points (Figure 4a) shows that the preferred quadrants correspond to the stable focus/stretching (*II*) ad the unstable node/saddle/saddle (*IV*) topologies. Also, the lines of constant PDF asymptote toward the δ-curve, which represents the tail of the tear-drop shaped (Q, R) distribution. The PDF sampled at $\tau_p^+ = 116.3$ particle positions (Figure 4b) occupies a relatively small area, centered around the origin of the (Q, R)-plane, indicating that larger particles tend to avoid the strongest vortical regions (*I* and *II* quadrants in Figure 3) as well as the *IV* quadrant of Figure 3. Only convergence regions (*III* quadrant in Figure 3) seem to be little affected by the preferential sampling of these particles. These observations do not hold for the $\tau_p^+ = 29.1$ particles (Figure 4c),

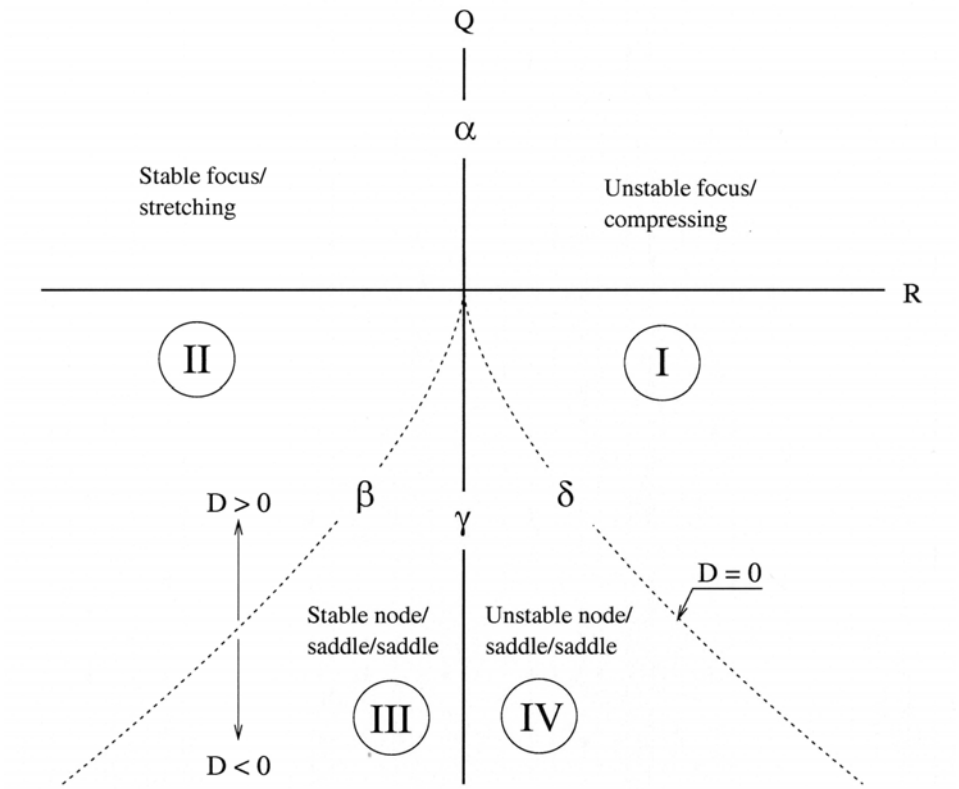

Figure 3 Incompressible flow critical point topologies according to the classification scheme of Chong *et al.* [18].

characterized by a broader PDF which would suggest a behaviour similar to that of fluid particles in the proximity of the wall. The PDF sampled at $\tau_p^+ = 3.8$ particle positions (Figure 4d) indicates an intermediate behaviour. Results obtained by Rouson & Eaton [15] for the PDF sampled at particle position are qualitatively similar despite some differences from a quantitative viewpoint. Discrepancies may be due to several causes: we simulated a turbulent upflow (not downflow as Rouson & Eaton) and considered the effect of Saffman lift force on particles with relaxation times different from those investigated by Rouson & Eaton.

The topological analysis seems to suggest that, very near the wall, "strongly coherent vortical structures are depleted of particles as would be if the local flow is producing particle non-homogeneous concentration" [15]. This result is relevant and yet it gives little specific information about the wall regions where particle build-up occurs. To identify these regions we need a different identification criterion.

To this aim, we can observe that, for incompressible flow, the fluctuating part, $u'_{i,j}$, of the velocity gradient tensor computed at the wall has the following form:

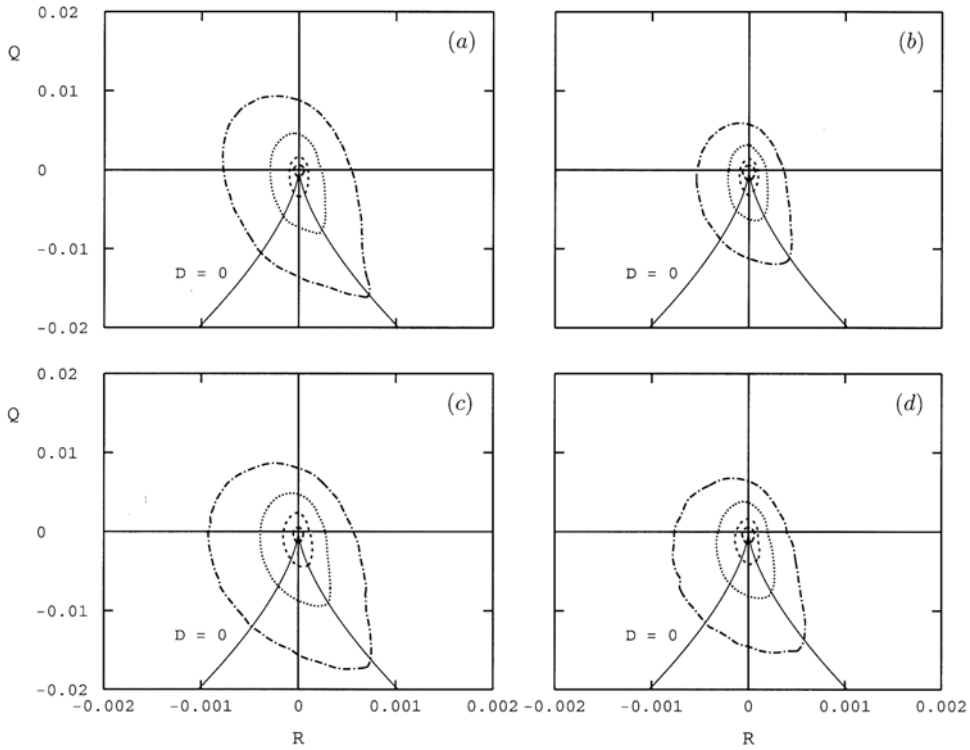

Figure 4 Viscous sublayer ($z^+ < 5$) joint PDF of *Q, R* conditionally sampled for fluid at grid points (a), at $\tau_p^+ = 116.3$ particle positions (b), at $\tau_p^+ = 29.1$ particle positions (c), and at $\tau_p^+ = 3.8$ particle positions (d). Isoline values are: —— PDF = 10, --- PDF = 1, ··· PDF = 0.1, – · – PDF = 0.01.

$$u'_{i,j}\big|_w = \begin{pmatrix} 0 & 0 & \partial u' / \partial z\big|_w \\ 0 & 0 & \partial v' / \partial z\big|_w \\ 0 & 0 & 0 \end{pmatrix},$$

and the following identities are true: $\tau'_{yz}\big|_w = \mu \cdot \partial v'/\partial z\big|_w$ and $\tau'_{xz}\big|_w = \mu \cdot \partial u'/\partial z\big|_w$. We already pointed out that the low speed streaks are ejection-like environments that correlate with lower-than-mean wall shear stress regions, where $\tau'_{xz}\big|_w < 0$, and appear much wider than high speed streaks, associated with higher-than-mean wall shear stress regions, where $\tau'_{xz}\big|_w > 0$. We exploited the relationship between the wall shear stress and the elements of the velocity gradient computed at the wall to describe the near-wall flow regions where particle build-up occurs.

In Figure 5, we show the instantaneous joint correlations of non-zero components of $u'_{i,j}|_w$. We considered the correlations for the fluid (sampled at grid points) and for $\tau_p^+ =$ 3.8, 29.1 and 116.3 particles (sampled at particle positions). Correlations were computed as follows: (i) we considered only the position of particles located in the viscous sublayer – i.e. at $z^+ < 5$; (ii) we projected each particle position onto the wall; (iii) we computed the components of $u'_{i,j}$ at the projected wall location. We can observe two distinct near-wall flow regions: with respect to the wall-normal direction, we identify a sweep-like inflow region, characterized by $\tau'_{yz}|_w = 0$ and by $\tau'_{xz}|_w > 0$, and an ejection-like outflow region, characterized by $\tau'_{yz}|_w = 0$ and by $\tau'_{xz}|_w < 0$. Correlations shown in Figures 5b, 5c and 5d demonstrate that, regardless of particle size, particles in the viscous sublayer tend to accumulate in proximity of wall regions characterized by negative values of $\tau'_{xz}|_w$, i.e. by negative values of $\partial u'/\partial z|_w$: 61% of the $\tau_p^+ = 3.8$ particles,

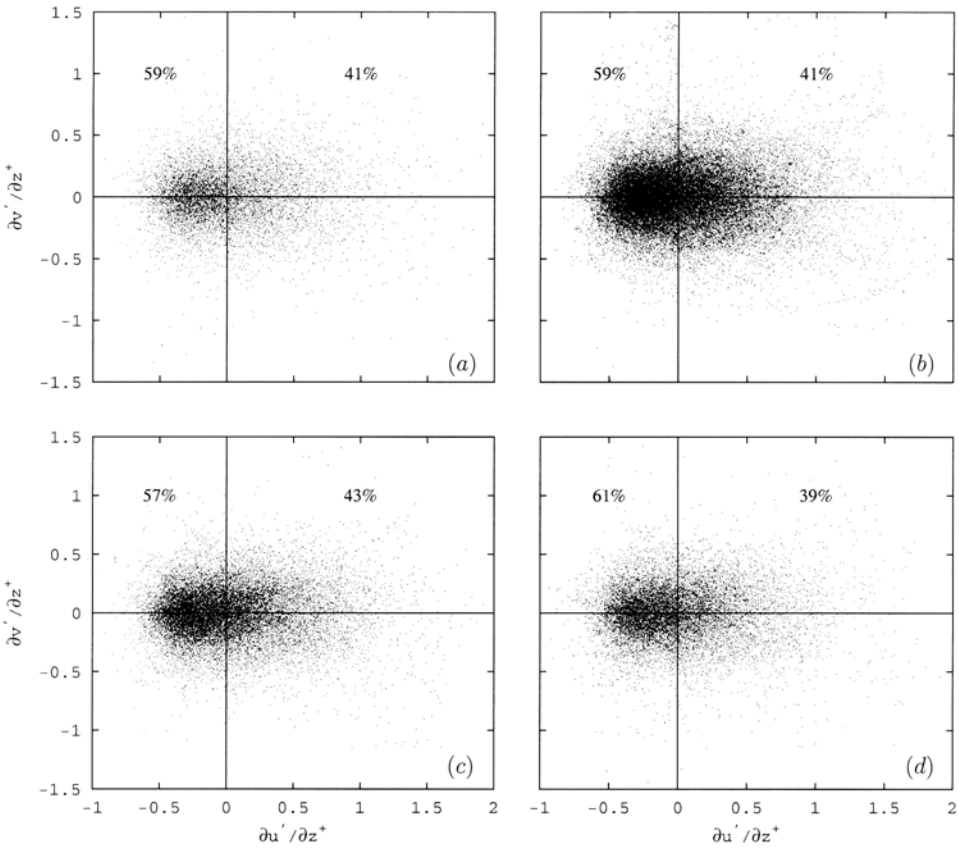

Figure 5 Viscous sublayer ($z^+ < 5$) instantaneous joint correlations of non-zero components of the fluctuating strain tensor, conditionally sampled for the fluid at grid points (a), $\tau_p^+ = 116.3$ particle positions (b), at $\tau_p^+ = 29.1$ particle positions (c), and at $\tau_p^+ = 3.8$ particle positions (d). Joint correlations demonstrate that particles are mostly concentrated in the ejection-like environments. The percentage indicates the number of particles in a region of positive/negative $\partial u'/\partial z|_w$.

57% of the $\tau_p^+ = 29.1$ particles and 59% of the $\tau_p^+ = 116.3$ particles fall in the $\partial u'/\partial z|_w < 0$ quadrants.

Even the fluid (see Figure 5a) shows a preferential distribution in such quadrants. This behavior can be explained by considering the mechanisms by which the low-speed streaks are generated: as shown in Figure 2, a jet of fluid which is directed to the wall generates the sweep and also the high speed region; then the jet of fluid, by continuity, is deflected by the wall and generates the low-speed ejection. Due to the entrainment of surrounding fluid, the sweep is more intense and concentrated and the following ejection spreads over a wider cross-section and has lower momentum. Low-sped, low-shear regions, where $\tau'_w < 0$ (i.e. $\partial y'/\partial z^+|_w < 0$), appear much wider than high-speed high-shear regions, where $\tau'_w > 0$ (i.e. $\partial u'/\partial z^+|_w > 0$). Thus, grid points necessarily sample $\partial u'/\partial z^+|_w < 0$ regions more often than $\partial u'/\partial z^+|_w > 0$ regions. However, in the latter regions, sampling at grid points appears more scattered and cover a wider range of values of $\partial u'/\partial z^+|_w$.

The correlations shown in figure 5 are similar for all of the 400 instants of the flow field we studied This result, together with the fact that the preferred wall regions are also characterized by values of $\partial v'/\partial z|_w$ nearly equal to zero, indicates that particle concentration build-up in the viscous sublayer occurs preferentially in the proximity of a near-wall outflow region. This can be explained considering the crucial role of the quasi-streamwise vortices in trapping particles very near the wall ([1]).

Similar conclusions were drawn from further analysis on particle behaviour in absence of gravity, as shown in table 1, where we report the statistics of the correlation between particle position and $\partial u'/\partial z|_w$ for two different flow configurations: upward channel flow (gravity directed downward) and channel flow with no gravity acting on particles. Again, $\partial u'/\partial z|_w < 0$ represents near-wall ejection-like regions where $\partial u'/\partial z|_w > 0$ represents near-wall sweep-like regions. For both flow configurations, particles tend to attain a preferential distribution in the ejection-like outflow regions. The comparison of the upflow case with the no-gravity case would suggest that preferential accumulation of different size particles in the viscous sublayer is not much affected by body forces applied on particles, at least for the particle sizes considered.

Table 1 Probabilities representing the correlations between particle position and $\partial u'/\partial z|_w$. Probabilities are averaged over 400 instants of the flow field.

	Upflow		*No Gravity*	
τ_p^+	$\left.\frac{\partial u'}{\partial z}\right\|_w < 0$	$\left.\frac{\partial u'}{\partial z}\right\|_w > 0$	$\left.\frac{\partial u'}{\partial z}\right\|_w < 0$	$\left.\frac{\partial u'}{\partial z}\right\|_w < 0$
3.8	61%	39%	60%	40%
29.1	57%	43%	59%	41%
116.3	59%	41%	59%	41%

To provide a unifying pictorial view of the mechanisms discussed in this paper by statistical means, in Figure 6 we show the instantaneous snapshot of particle distribution and turbulent coherent structures in the near-wall region of the channel, superimposed to the local and instantaneous streamlines. Here, we focus on a $y - z$ window of the computational domain extruded for the length of one streamwise cell. Green and red surfaces represent counterclockwise and clockwise vortices respectively. The large-scale green vortex is generating a strongly coherent sweep on its downwash side and a strongly coherent ejection on its upwash side. Black circles represent particles going toward the wall within the sweep, blue circles represent particles going away from the wall, within the ejection. The action of the green vortex in transferring these particles is apparent.

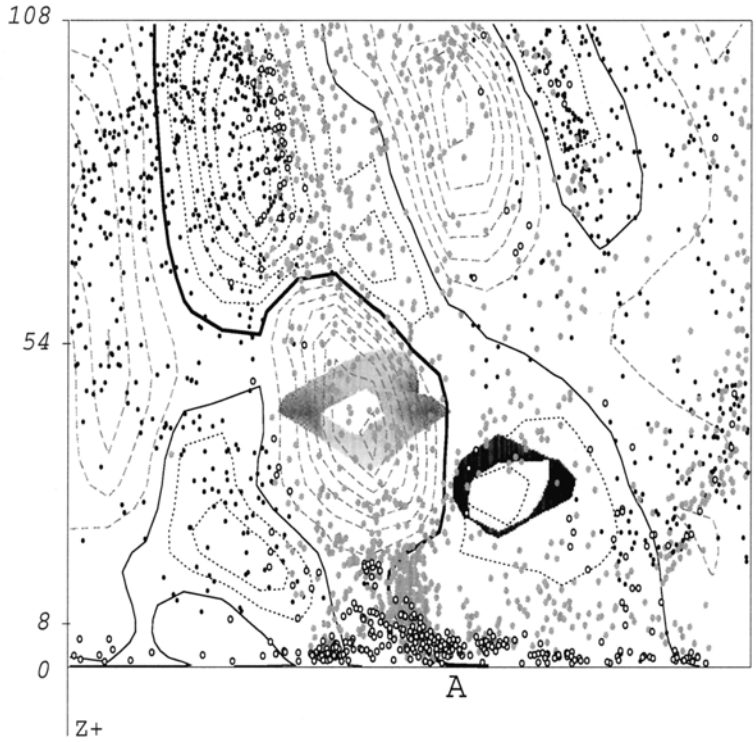

Figure 6 Instantaneous $y - z$ window of the computational domain extruded for the length of one streamwise cell showing a snapshot of particle distribution and turbulence coherent structures in the near-wall region with superimposed streamlines of channel flow. Green and red surfaces represent counterclockwise and clockwise vortices respectively. Large-scale green vortex is generating a strongly coherent sweep on its down-wash side and a strongly coherent ejection on its upwash side. Black circles represent particles going toward the wall within the sweep, blue circles represent particles going away from the wall, within the ejection. Vortices are separated by the $\Psi = 0$ streamline (thick black line) touching the wall in A and separating counterclockwise rotating region (left) and clockwise rotating region (right). Particles with negligible wall-normal velocity ($|w_P| < 10^{-3}$) are plotted as empty circles.

The two vortices are separated by the $\Psi = 0$ streamline (thick black line) touching the wall in A and separating the counterclockwise rotating region (left) from the clockwise rotating region (right). The flow region neighbouring the streamline is an ejection-like outflow region, characterized by low values of the wall shear-stress ($\partial u'/\partial z^+|_w < 0$). As reported in [1], this region is squeezed by the two vortices, thus reducing the probability that a particle is re-entrained into the outer flow. Particles with almost zero wall-normal velocity ($|w_P| < 10^{-3}$), plotted as empty circles, accumulate in the ejection-like region and remain trapped between the red vortex and the wall. It is also apparent that coherent vortices are not able to entrain those particles accumulated close to the wall. Events shown in Figure 6 have been observed in a large number of instants at different locations of the channel.

3. CONCLUSIONS

The work reported here is part of a program aimed at understanding and characterizing the interactions between coherent structures and inertial particles in boundary layer turbulence. Results shown here confirm the preferential accumulation of particles and the influence of turbulent structures. Once segregated in the wall region, inertial particles have a highly non-uniform distribution which peaks in the viscous sublayer, far from the strong coherent vortical structures. We computed the viscous sublayer instantaneous joint correlations of the non-zero components of the fluctuating velocity gradient tensor, and found that particles accumulate in ejection-like outflow regions Quantitative results presented here support evidence of the trapping mechanisms we described from a qualitative viewpoint in previous works [1, 2].

Financial support from MIUR under Grant n.RBAU012FRS (FIRB program) and Grant n.2003099224_002 (PRIN program), and from Regione Friuli Venezia-Giulia under Grant *Fluidodinamica e Analisi delle Dispersioni nella Bassissima Atmosfera del Friuli Venezia Giulia.* C.M. thankfully acknowledges Regione Friuli Venezia-Giulia for financial support under Grant PORO3 FVG 2000-2006 – Asse D – Misura D4.

NOMENCLATURE

Symbols

Fluid:

h	channel half-width	[m]
Re_τ	shear Reynolds number	
u_τ	shear velocity	[ms^{-1}]
u, v, w	velocity components	[ms^{-1}]
P, Q, R	invariants of the velocity gradient tensor	
$\tau_{x,z}$, τ_{yz}	shear stress	[$\mathrm{N{\cdot}m}^{-2}$]
μ	dynamic viscosity	[Pa·s]

Particles:

τ_p	relaxation time	[s]
D_p	diameter	[m]

Other symbols:

x, y, z	cartesian coordinates	[m]
t	time	[s]
+	non-dimensional units	

REFERENCES

1. Marchioli, C. and Soldati, A. (2002) Mechanisms for particle transfer and segregation in turbulent boundary layer, *J. Fluid Mech*., vol. 468, pp. 283-315.
2. Marchioli, C., Giusti, A., Salvetti, M. V. and Soldati, A. (2003) Direct numerical simulation of particle wall transfer and deposition in upward turblent pipe flow, *Int. J. Multiphase Flow*, vol. 29, pp. 10107-1038.
3. Marchioli, C., Picciotti, M. and Soldati, A. (2004) Interactions between turbulence structure and inertial particles in boundary layers: mechanisms for particle transfer and preferential distribution, in *Modelling and Experimentation in two-phase flow*, (ed. V. Bertola), CISM Courses and Lectures, vol. 450, pp. 383-434, Springer.
4. Pedinotti, S., Mariotti, G. and Banerjee, S. (1992) Direct numerical simulation of particle behavior in the wall region of turbulent flow in horizontal channels, *Int. J. Multiphase Flow,* vol. 18, pp. 927-941.
5. Niño, Y. and Garcia, M. H. (1996) Experiments on particle-turbulence interactions in the near-wall region of an open channel flow: implication for sediment transport, *J. Fluid Mech.*, vol. 326, pp. 285-319.
6. Zhang, H. and Ahmadi, G. (2000) Aerosol particle transport and deposition in vertical and horizontal turbulent duct flow, *J. Fluid Mech.*, vol. 387, pp. ;353-396.
7. Reeks, M. W. (1983) The transport of discrete particles in inhomogeneous turbulence, *J. Aerosol Sci.*, vol. 310, pp. 729-739.
8. Brooke, J. W., Kontomaris, K., Hanratty, T. J. and McLaughlin, J. B. (1992) Turbulent deposition and trapping of aerosols at a wall, *Phys. Fluids A,* vol. 14, pp. 825-834.
9. Narayanan, C., Lakehal, D., Botto, L. and Soldati, A. (2003) Mechanisms of particle deposition in a fully developed turbulent channel flow, *Phys. Fluids A,* vol. 15, pp. 763-775.
10. Adrian, R. J., Meinhart, C. D. and Tomkins, C. D. (2000) Vortex organization in the outer region of the turbulent boundary layer. *J. Fluid Mech.*, vol. 422, pp. 1-54.
11. Schoppa, W. and Hussain, F. (2003) Coherent structures generation in near the wall turbulence. *J. Fluid Mech.*, vol. 453, pp. 57-108.
12. Jimenez, J. and Pinelli, A. (1999) The autonomous cycle of near-wall turbulence. *J. Fluid Mech.*, vol. 389, pp. 335-359.

13. Jeong, J., Hussain, F., Schoppa, W. and Kim, J. (1997) Coherent structures near the wall in a turbulent channel flow. *J. Fluid Mech.*, vol. 332, pp. 185-214.
14. Cleaver, J. W. and Yates, B. (1975) A sub layer model for the deposition of particles from a turbulent flow, *Chem. Eng. Sci.*, vol. 30, pp. 983-992.
15. Rouson, D. W. and Eaton, J. K. (2001) On the preferential concentration of solid particles in turbulent, *J. Fluid Mech.*, vol. 428, pp. 149-169.
16. Kaftori, D., Hetsroni, G. and Banerjee, S. (1995) Particle behavior in the turbulent boundary layer. II. Velocity and distribution profiles, *Phys. Fluids A*, vol. 7, pp. 1107-1121.
17. Pan, Y. and Banerjee, S. (1996) Numerical simulation of particle interactions with wall tubuence, *Phys. Fluids A,* vol. 8, pp. 2733-2755.
18. Chong, M. S., Perry, A. and Cantwell, B. J. (1990) A general classification of three-dimensional flow fields, *Phys. Fluids A*, vol. 2, pp. 765-777.
19. Blackburn, H. M., Mansour, N. N. and Cantwell, B. J. (1996) Topology of fine-scale motions in turbulent channel flow, *J. Fluid Mech.*, vol. 310, pp. 269-292.
20. Jeong, J. and Hussain, F. (1995) On the identification of a vortex. *J. Fluid Mech.*,. vol. 285, pp. 69-94.